

# Electronic structure, self-doping, and superconducting instability in the alternating single-layer trilayer stacking nickelates $\text{La}_3\text{Ni}_2\text{O}_7$

Yang Zhang,<sup>1</sup> Ling-Fang Lin,<sup>1</sup> Adriana Moreo,<sup>1,2</sup> Thomas A. Maier,<sup>3</sup> and Elbio Dagotto<sup>1,2</sup>

<sup>1</sup>*Department of Physics and Astronomy, University of Tennessee, Knoxville, Tennessee 37996, USA*

<sup>2</sup>*Materials Science and Technology Division, Oak Ridge National Laboratory, Oak Ridge, Tennessee 37831, USA*

<sup>3</sup>*Computational Sciences and Engineering Division,  
Oak Ridge National Laboratory, Oak Ridge, Tennessee 37831, USA*

(Dated: April 26, 2024)

Motivated by the recently proposed alternating single-layer trilayer stacking structure for the nickelate  $\text{La}_3\text{Ni}_2\text{O}_7$ , we comprehensively study this system using *ab initio* and random-phase approximation techniques. Our analysis unveils similarities between this novel  $\text{La}_3\text{Ni}_2\text{O}_7$  structure and other Ruddlesden-Popper nickelate superconductors, such as a similar charge-transfer gap value and orbital-selective behavior of the  $e_g$  orbitals. However, different from other Ruddlesden-Popper nickelate superconductors, we do not observe any obvious reconstruction of the Fermi surface from ambient conditions (Cmmm phase) to high pressures (P4/mmm phase). Pressure primarily increases the bandwidths of the Ni  $e_g$  bands, suggesting an enhancement of the itinerant properties of those  $e_g$  states. Furthermore, the  $d_{3z^2-r^2}$  orbital also has a layer-selective behavior because the antibonding-bonding-nonbonding splitting can only be obtained in the trilayer. In addition, we observe a “self-doping” effect from the trilayer to the single-layer sublattices and this effect will be enhanced by overall electron doping. Moreover, we find a leading  $d_{x^2-y^2}$ -wave pairing state that is restricted to the single-layer. Because the effective coupling between the single layers is very weak – due to the non-superconducting trilayer in between – this suggests that the superconducting transition temperature  $T_c$  in this structure should be much lower than in the bilayer structure.

*Introduction.*– The Ruddlesden-Popper (RP) perovskite nickelate systems have recently attracted considerable attention due to the discovery of superconductivity under pressure in  $\text{La}_3\text{Ni}_2\text{O}_7$  (327-LNO) with a  $d^{7.5}$  configuration [1], opening a remarkable and challenging avenue for the study of nickelate-based unconventional high- $T_c$  superconductivity [2–7].

For the 327-LNO system, the original experiments reported a bilayer (BL) stacking structure [1], where superconductivity was found in a very broad pressure range, with a high transition temperature up to 80 K [1]. This occurs after a first-order structural transition from the ambient-pressure Amam phase with distorted  $\text{NiO}_6$  octahedra to the high-pressure Fmmm phase without tilting of those oxygen octahedra (see Fig. 1(a)). Based on the BL structure, many follow-up experimental [8–13] and theoretical [14–35] efforts were presented to understand the interesting physical properties and possible superconducting pairing mechanism in this compound. Very recently, J. Li *et al.* [36] observed the Meissner effect of the superconducting state using the *ac* magnetic susceptibility, with the superconducting volume fraction being around 50%.

Furthermore, an interesting alternating single-layer (SL) – trilayer (TL) stacking structure was proposed experimentally (with the same chemical formula 327-LNO) as an alternative to the BL stacking structure (see Fig. 1(a)), by several groups [37–40]. Interestingly, signatures of superconductivity under pressure were also reported in another RP nickelate  $\text{La}_4\text{Ni}_3\text{O}_{10}$  with only a trilayer stacking structure [41–47]. However,

superconductivity was absent in SL  $\text{La}_2\text{NiO}_4$  under pressure [6].

Similarly to 327-LNO (BL), the corner-sharing  $\text{NiO}_6$  octahedra were also found to be strongly distorted in TL  $\text{La}_4\text{Ni}_3\text{O}_{10}$  at ambient conditions [41–47], leading to a monoclinic  $\text{P}2_1/c$  structure (No. 14). Increasing pressure suppresses the distortion of the  $\text{NiO}_6$  octahedra, yielding a high-symmetry  $\text{I}4/\text{mmm}$  phase without the tilting of oxygen octahedra around 15 GPa, where the signature of superconductivity was found with a  $T_c$  of about 20 – 30 K [43–47]. However, in 327-LNO (SL-TL), the  $\text{NiO}_6$  oxygen octahedra do not display any substantial tilting in neither the ambient-pressure Cmmm nor the high-pressure  $\text{P}4/\text{mmm}$  phases [37–39].

Considering these developments, several interesting questions naturally arise: What are the similarities and differences between the 327-LNO (SL-TL) and other RP nickelate superconductors under pressure? What interesting physics can be obtained in this alternating SL and TL stacking 327-LNO, as compared to the first proposed bilayer 327-LNO structure? Could we obtain superconductivity in 327-LNO (SL-TL) and is the pairing mechanism the same as in other RP nickelate superconductors?

*Electronic structure of 327-LNO (SL-TL)* – In the 327-LNO (BL) system, due to the “dimer” physics induced by its bilayer geometry [15], the  $d_{3z^2-r^2}$  orbital splits into antibonding and bonding states, while the  $d_{x^2-y^2}$  orbital remains decoupled among planes, as shown in Fig. 1(b), resulting in an orbital-selective behavior [48, 49]. Considering the nominal valence  $\text{Ni}^{2.5+}$ , close to two electrons would occupy the bonding states of the

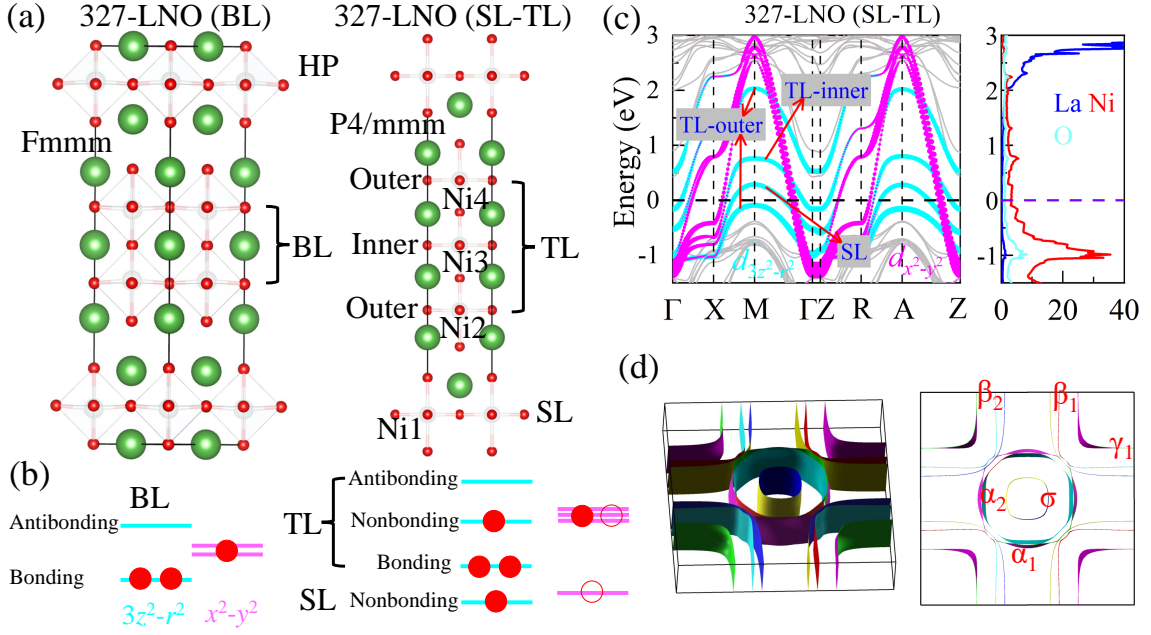


FIG. 1. (a) Schematic crystal structure of the conventional cells of the high-pressure Fm $\bar{3}$ mm phase of 327-LNO (BL) and P4/mmm phase of 327-LNO (SL-TL), respectively (green = La; gray = Ni; red = O). All crystal structures were visualized using the VESTA code [55]. (b) Sketches of electronic states in the BL and SL-TL. The light blue (pink) horizontal lines represent  $d_{3z^2-r^2}$  ( $d_{x^2-y^2}$ ) states. The solid and open circles represent 1.0 and 0.5 electrons, respectively. The total population of  $e_g$  electrons considered is  $n = 3.0$  and  $n = 6.0$  electrons, for BL with two sites and SL-TL with four sites, respectively. (c) The Ni  $e_g$ -orbitals projected band structures and density of states. The  $d_{3z^2-r^2}$  and  $d_{x^2-y^2}$  orbitals are distinguished by the blue and red lines. (d) FS for the non-magnetic state of the high-pressure P4/mmm phase of the 327-LNO (SL-TL) structure at 16 GPa. Note that the local  $z$ -axis is perpendicular to the NiO $_6$  plane towards the top O atom, while the local  $x$ - or  $y$ -axis is along the in-plane Ni-O bond directions.

$d_{3z^2-r^2}$  orbital and approximately one electron stays in the  $d_{x^2-y^2}$  band [15] (see Fig. 1(b)).

Because 327-LNO (SL-TL) has an alternating SL and TL stacking structure, the  $d_{3z^2-r^2}$  orbital from the TL sublattice also splits into antibonding, nonbonding, and bonding states due to the “trimer” physics induced by the TL structure [50], as displayed in Fig. 1(b). Meanwhile, the  $d_{x^2-y^2}$  orbital does not participate in the formation of antibonding and bonding states, as well as the  $e_g$  states from the SL sublattice. Considering an average of 1.5 electrons in  $e_g$  states per Ni in the 327-LNO, two electrons would occupy the bonding states of the  $d_{3z^2-r^2}$  orbital and one electron enters the nonbonding state in the TL sublattice, while an extra 1.5 electrons would remain in the  $d_{x^2-y^2}$  state [Fig. 1(b)]. For the SL sublattice, 1.0 and 0.5 electrons would occupy the states of the  $d_{3z^2-r^2}$  and  $d_{x^2-y^2}$  orbitals, respectively. Being a SL, these are, obviously, only nonbonding states. Then, the  $e_g$  orbitals of 327-LNO (SL-TL) have both orbital-selective and layer-selective characteristics.

To better understand the physical properties of 327-LNO (SL-TL), we have calculated the electronic structure based on the experimental crystal structure under pressure [56] using first-principles density functional theory (DFT) [51–54]. The states near the

Fermi level mainly arise from Ni  $3d$  orbitals hybridized with O  $p$ -states, which are located at lower energies than the Ni  $3d$  states, indicating a charge-transfer picture similar to other nickelates [15, 30, 59]. As expected, the  $d_{3z^2-r^2}$  orbital from the TL sublattice splits into three antibonding, nonbonding, and bonding related bands in the 327-LNO (SL-TL) band structure, as shown in Fig. 1(c). In addition, the  $d_{x^2-y^2}$  orbital from the TL sublattice and the  $e_g$  orbitals from the SL sublattice all remain nearly decoupled between different planes.

Similarly as it occurs in 327-LNO (BL), due to the strong in-plane hybridization of the  $e_g$  states [15] electrons transfer between the  $d_{3z^2-r^2}$  and  $d_{x^2-y^2}$  orbitals in 327-LNO (SL-TL) as well, leading to a noninteger electronic population in both orbitals. A crucial observation is that different from the TL La $_4$ Ni $_3$ O $_{10}$ , the bonding band of the  $d_{3z^2-r^2}$  states from the TL sublattice *does not touch* the Fermi surface (FS). Therefore, the TL states do not create a Fermi surface  $\gamma$  pocket in 327-LNO (SL-TL) (see Fig. 1(d)). Instead, a  $\gamma$  pocket does exist in the TL La $_4$ Ni $_3$ O $_{10}$  context [50], basically due a different crystal field. Note that the  $\gamma_1$  sheet shown in Fig. 1(d) arises *entirely* from the SL sublattice, and should not be confused with the  $\gamma$  pocket of the BL and TL systems. The TL sublattice states give

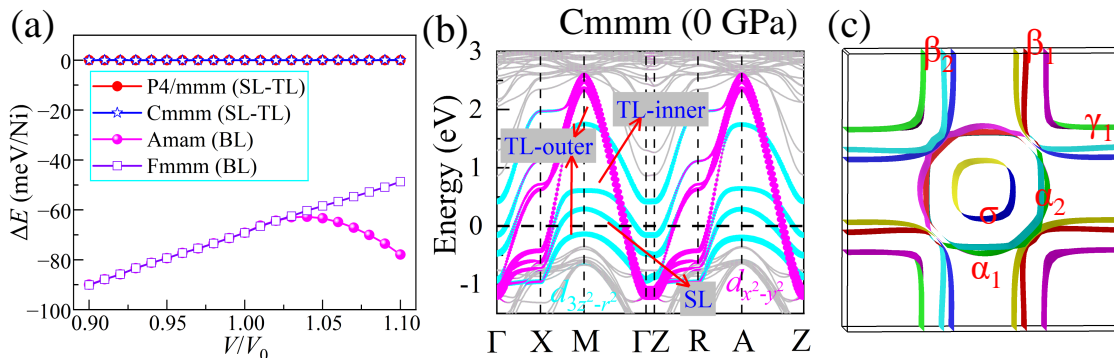


FIG. 2. (a) Calculated energies of different structural phases of 327-LNO (SL-TL) and 327-LNO (BL), as a function of the ratio  $V/V_0$ . Here,  $V_0$  is the conventional-cell volume of the P4/mmm phase of 327-LNO (SL-TL) at 16 GPa. The P4/mmm phase of 327-LNO (SL-TL) is taken as the energy of reference. (b) The Ni  $e_g$ -orbitals projected band structure. (c) Fermi surface for the non-magnetic state of the Cmmm phase of the 327-LNO (SL-TL) crystal structure without pressure.

rise to two  $\beta$  sheets and an  $\alpha_1$  sheet of mixed  $e_g$  orbital character, while the  $\sigma$  pocket is made up of the  $d_{3z^2-r^2}$  orbital in the 327-LNO (SL-TL), similar to  $\text{La}_4\text{Ni}_3\text{O}_{10}$ . Moreover, the SL sublattice also gives rise to the  $\alpha_2$  sheet displayed in Fig. 1(d).

*Pressure effect* – To understand better the different phases of 327-LNO (SL-TL) and 327-LNO (BL), we also studied the energies when changing the ratio  $V/V_0$ , where  $V_0$  is the conventional-cell volume of the P4/mmm phase of 327-LNO (SL-TL) at 16 GPa. As shown in Fig. 2(a), 327-LNO (BL) always has lower energy than 327-LNO (SL-TL) when changing the ratio  $V/V_0$  from 0.9 to 1.10. In addition, as the volume increases, corresponding to a decrease in pressure, the Amam phase has lower energy than the Fmmm phase in the 327-LNO (BL) structure, in agreement with a previous experiment [1]. For 327-LNO (SL-TL), the P4/mmm and Cmmm phases have nearly degenerate energies in the entire  $V/V_0$  region that we studied because the distortions from the high symmetry P4/mmm phase are quite small.

In addition, we calculated the electronic structure of the Cmmm phase of the 327-LNO (SL-TL) crystal structure based on the primitive unit cell, by using the experimental results without pressure. As displayed in Fig. 2(b), the band structure of the Cmmm phase looks quite similar to the P4/mmm phase under pressure. By comparing the band structures of the ambient and high-pressure cases, the bandwidths of the Ni  $e_g$  bands increase upon pressure by  $\sim 16\%$  at 16 GPa, suggesting an enhancement of itinerant properties of the  $e_g$  states. Furthermore, we also do not observe any obvious reconstruction of the FS between the P4/mmm and Cmmm phases, as displayed in Fig. 2(c). Taken together, all these results suggest that the structural phase transition Cmmm-P4/mmm should not induce the stabilization of superconductivity in 327-LNO (SL-TL).

*Tight-binding model and self-doping effect* – To understand the low-energy physics under pressure, we

constructed an eight-band  $e_g$ -orbital tight-binding model for the SL and TL sublattice states for the P4/mmm phase of 327-LNO (SL-TL) at 16 GPa, with overall filling  $n = 6$ , including the longer-range hoppings between the SL and TL sublattices. The entire hopping file used in the present work can be found in Supplementary Material [58], where additional details are provided for the tight-binding model.

As shown in Figs. 3(a) and (b), the tight-binding band structure and FS fit very well with the DFT results discussed in the previous section. By using the maximally localized Wannier functions (MLWFs) method based on the WANNIER90 package [60], we obtained the crystal-field splitting of the  $e_g$  orbitals for different Ni sites in the P4/mmm phase of 327-LNO (SL-TL), as summarized in Fig. 3(c). The Ni1 site from the SL sublattice has a larger crystal-field splitting ( $\Delta \sim 0.666$  eV) than the Ni2, Ni3, and Ni4 sites from the TL sublattice. In the TL sublattice, the outer layers (Ni2 and Ni4 sites) have lower on-site energies than the middle layer (Ni3 site), similarly to the case of the TL for  $\text{La}_4\text{Ni}_3\text{O}_{10}$ . Furthermore, we find that the ratios  $t^{12}/t^{22}$  are 0.425, 0.511, and 0.548 for the Ni1, Ni2/Ni4 and Ni3 sites, respectively (where the in-plane inter-orbital hopping between the  $d_{3z^2-r^2}$  and  $d_{x^2-y^2}$  orbitals is  $t^{12}$ , and the intra-orbital  $d_{x^2-y^2}$  hopping is  $t^{22}$ ). This indicates that the in-plane hybridization of the  $e_g$  orbitals is stronger in the TL sublattice.

Considering the average electronic density of the  $e_g$  states (1.5 per Ni) in 327-LNO (SL-TL), the calculated electronic densities are approximately 1.770, 1.436, and 1.360 for Ni1, Ni2/Ni4 and Ni3 sites, respectively. This indicates a “self-doping” effect, where electrons are transferred from the TL to the SL sublattice. Note that here the sum of the electronic populations of Ni2, Ni3, and Ni4 ( $\sim 4.23$ ), locates the system in the superconducting region of  $\text{La}_4\text{Ni}_3\text{O}_{10}$ , where  $d_{3z^2-r^2}$   $\gamma$  pockets are obtained according to Ref. [50]. The primary

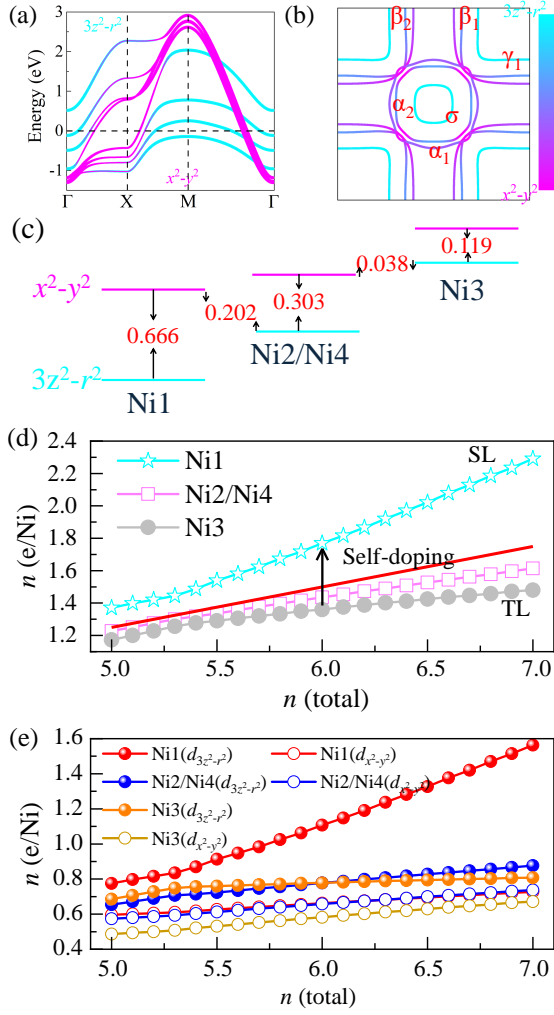


FIG. 3. (a) Tight-binding band structure and (b) Fermi surface for the P4/mmm phase of 327-LNO (SL-TL) at 16 GPa. Here, an eight-band  $e_g$  orbital tight-binding model was considered including SL and TL hoppings (see the hopping file in the Supplementary Material [58]) with an overall filling of  $n = 6$  (i.e. 1.5 electrons per site). (c) Crude sketches of the crystal-field splitting of the  $e_g$  orbitals for different Ni sites. All the values are given in units of eV. (d) The total electron occupations and (e) different electronic densities of the  $e_g$  orbitals for the different Ni sites vs. the overall filling  $n$  in the tight-binding model. The red line in panel (d) represents the average electronic Ni site occupancy.

intuitive reason why TL  $\text{La}_4\text{Ni}_3\text{O}_{10}$  has a  $\gamma$  pocket, and thus superconductivity, but TL from 327-LNO (SL-TL) does not, is because of the crystal-field value: it is larger in TL from 327-LNO (SL-TL) than in TL  $\text{La}_4\text{Ni}_3\text{O}_{10}$ .

Moreover, the outer Ni layers (Ni2 and Ni4 sites) of the TL sublattice have more electrons than the middle layer (Ni3 site). In addition, we also calculated the electron occupations for different Ni sites by changing the overall filling  $n$  from 5.0 to 7.0, as displayed in Figs. 3(d) and (e). For electronic doping, extra electrons move to the SL Ni1 site with an increased difference in electron

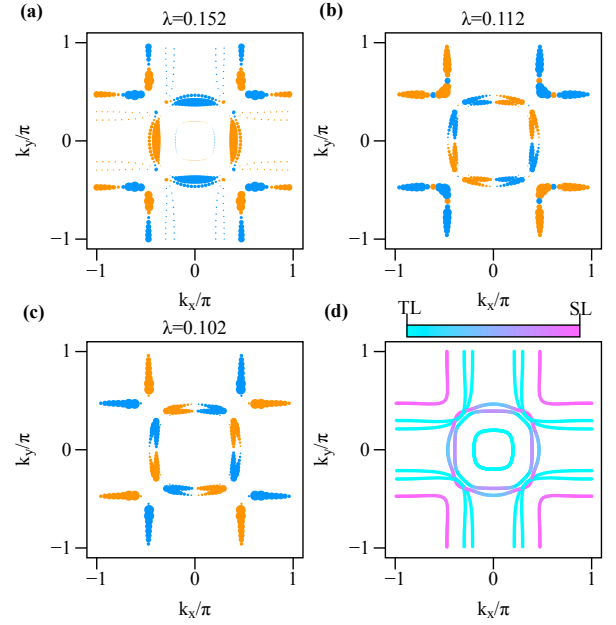


FIG. 4. The RPA calculated leading superconducting singlet gap structure  $g_\alpha(\mathbf{k})$  for momenta  $\mathbf{k}$  on the Fermi surface of 327-LNO (SL-TL) at  $n = 6.0$  and their pairing strength  $\lambda$ : (a) Leading  $d_{x^2-y^2}$ -wave state with  $\lambda = 0.152$ , (b) subleading  $d_{x^2-y^2}$ -wave state with  $\lambda = 0.112$ , (c)  $g$ -wave state with  $\lambda = 0.102$ . The sign of the gap structure  $g_\alpha(\mathbf{k})$  is indicated by the colors (orange = positive, blue = negative), and the gap amplitude by the point size. The RPA calculations used Coulomb interaction parameters  $U = 0.5$  (intra-orbital),  $U' = U/2$  (inter-orbital), and  $J = J' = U/4$  (Hund coupling and pair hopping, respectively) in units of eV. The hopping parameters are available in the Supplementary Material [58]. The dominant character of the Fermi surface Bloch states arising from the SL (magenta) and TL (cyan) sublattices is shown in panel (d).

densities between the SL and TL sublattices, suggesting an enhanced “self-doping” effect. Specifically, in the hole-doping region, the SL Ni1 site loses more electrons than other sites in the TL sublattice. As shown in Fig. 3(e), for the doping region we studied, the electronic occupation of the  $d_{3z^2-r^2}$  orbitals is larger than that in the  $d_{x^2-y^2}$  orbital.

*RPA pairing tendencies* – To analyze the superconducting pairing tendencies, we used multi-orbital random phase approximation (RPA) calculations to assess the tight-binding model including the SL and TL sublattices. The RPA calculations of the pairing vertex are based on a perturbative weak-coupling expansion in the local Coulomb interaction matrix, which contains intra-orbital ( $U$ ), inter-orbital ( $U'$ ), Hund’s rule coupling ( $J$ ), and pair hopping ( $J'$ ) terms [61–64]. The pairing strength  $\lambda_\alpha$  for pairing channel  $\alpha$  and its corresponding pairing structure  $g_\alpha(\mathbf{k})$  are obtained by

solving an eigenvalue problem of the form

$$\int_{FS} d\mathbf{k}' \Gamma(\mathbf{k} - \mathbf{k}') g_{\alpha}(\mathbf{k}') = \lambda_{\alpha} g_{\alpha}(\mathbf{k}), \quad (1)$$

where the momenta  $\mathbf{k}$  and  $\mathbf{k}'$  are restricted to the FS, and  $\Gamma(\mathbf{k} - \mathbf{k}')$  is the irreducible particle-particle vertex. In the RPA approximation, the dominant term entering  $\Gamma(\mathbf{k} - \mathbf{k}')$  is the RPA spin susceptibility  $\chi_s(\mathbf{k} - \mathbf{k}')$ .

By solving the eigenvalue problem in Eq. 1 for the RPA calculated pairing vertex  $\Gamma(\mathbf{k} - \mathbf{k}')$  of 327-LNO (SL-TL) at  $n = 6.0$ , we find that the  $d_{x^2-y^2}$  channel is the leading pairing instability caused by spin fluctuations, followed by subleading  $d_{xy}$ - and  $g$ -wave solutions, as displayed in Figs. 4(a-c). Here we used  $U = 0.5$  eV,  $U' = U/2$ ,  $J = J' = U/4$ . We find that larger  $U$  causes a spin-density wave instability in the SL sublattice with  $\mathbf{q} \sim (\pi, \pi, 0)$  arising from the near perfect nesting of the SL  $\alpha_2$  and  $\gamma_1$  sheet Fermi surface states (magenta regions in Fig. 4(d)). Despite the small value of  $U$ , the pairing strength  $\lambda = 0.152$  of the leading  $d_{x^2-y^2}$  state is already significant. As a comparison, for the bilayer 327 structure, we obtained  $\lambda \sim 0.2$  at 15 GPa for  $U = 0.8$  eV [21]. Moreover, we note that for all three leading pairing states, the pairing gap is only finite on the regions of the Fermi surface made up of states from the SL sublattice (magenta regions in panel (d) in Fig. 4), and negligible in the TL dominated regions. This suggests that pairing, while strong, is restricted to the SL sublattice, and caused by strong intra-SL-sublattice spin fluctuations between the  $\alpha_2$  and  $\gamma_1$  Fermi surface sheets. We believe that it is the absence of a TL  $\gamma$ -pocket that pairing in the TL sublattice is weak. Based on these results, we speculate that a possible three-dimensional superconducting transition involving the SL system would be suppressed to very low temperatures, because the effective coupling between different SL sublattices is negligible due to the presence of the TL in between.

*Conclusions.* – In summary, we presented a systematic study of the newly reported 327-LNO (SL-TL), with an alternating single-layer and trilayer stacking structure, by using DFT and RPA calculations. We found a large charge-transfer energy, a common character with other nickelates. In addition, more importantly, we did not observe any obvious reconstruction of the Fermi surface from the ambient-pressure Cmmm to the high-pressure P4/mmm phases. By changing the volume ratio  $V/V_0$  from 0.9 to 1.10, corresponding to the effect of pressure, we found that 327-LNO (BL) always has lower energy than 327-LNO (SL-TL). Furthermore, the  $e_g$  orbitals of 327-LNO (SL-TL) have both orbital-selective and layer-selective behaviors. Moreover, we observed a “self-doping” effect from the TL to the SL sublattice, which is enhanced by electron doping. Based on RPA calculations, we obtained a leading  $d_{x^2-y^2}$ -wave pairing state with sizable pairing strength  $\lambda$ . However, this pairing state is restricted to the SL sublattice and,

therefore, a three-dimensional superconducting state will be suppressed to very low temperatures due to the weak coupling between the SL sublattices, which will reduce the coherence between those layers. These results suggest that a possible superconducting  $T_c$  in 327-LNO (SL-TL) may not be sufficiently high to match the experimentally observed  $T_c$  in 327-LNO. Consequently, we believe that a bilayer stacking structure remains the most likely in 327-LNO with  $T_c \sim 80$  K.

This work was supported by the U.S. Department of Energy (DOE), Office of Science, Basic Energy Sciences (BES), Materials Sciences and Engineering Division.

- 
- [1] H. Sun, M. Huo, X. Hu, J. Li, Y. Han, L. Tang, Z. Mao, P. Yang, B. Wang, J. Cheng, D.-X. Yao, G.-M. Zhang, and M. Wang, *Nature* **621** 493 (2023).
  - [2] Z. Liu, M. Huo, J. Li, Q. Li, Y. Liu, Y. Dai, X. Zhou, J. Hao, Y. Lu, M. Wang, and W.-H. Wen, *arXiv 2307.02950* (2023).
  - [3] Y. Zhang, D. Su, Y. Huang, H. Sun, M. Huo, Z. Shan, K. Ye, Z. Yang, R. Li, M. Smidman, M. Wang, L. Jiao, and H. Yuan, *arXiv 2307.14819* (2023).
  - [4] J. Hou, P. T. Yang, Z. Y. Liu, J. Y. Li, P. F. Shan, L. Ma, G. Wang, N. N. Wang, H. Z. Guo, J. P. Sun, Y. Uwatoko, M. Wang, G.-M. Zhang, B. S. Wang, and J.-G. Cheng, *arXiv 2307.09865* (2023).
  - [5] J. Yang, H. Sun, X. Hu, Y. Xie, T. Miao, H. Luo, H. Chen, B. Liang, W. Zhu, G. Qu, C.-Q. Chen, M. Huo, Y. Huang, S. Zhang, F. Zhang, F. Yang, Z. Wang, Q. Peng, H. Mao, G. Liu, Z. Xu, T. Qian, D.-X. Yao, M. Wang, L. Zhao, and X. J. Zhou, *arXiv 2309.01148* (2023).
  - [6] M. Zhang, C. Pei, Q. Wang, Y. Zhao, C. Li, W. Cao, S. Zhu, J. Wu, and Y. Qi, *arXiv 2309.01651* (2023).
  - [7] G. Wang, N. N. Wang, X. L. Shen, J. Hou, L. Ma, L. F. Shi, Z. A. Ren, Y. D. Gu, H. M. Ma, P. T. Yang, Z. Y. Liu, H. Z. Guo, J. P. Sun, G. M. Zhang, S. Calder, J.-Q. Yan, B. S. Wang, Y. Uwatoko, and J.-G. Cheng, *Phys. Rev. X* **14** 011040 (2024).
  - [8] M. Kakoi, T. Oi, Y. Ohshita, M. Yashima, K. Kuroki, Y. Adachi, N. Hatada, T. Uda, H. Mukuda, *arXiv 2312.11844* (2023).
  - [9] Z. Dong, M. Huo, J. Li, J. Li, P. Li, H. Sun, Y. Lu, M. Wang, Y. Wang, and Z. Chen, *arXiv 2312.15727* (2023).
  - [10] T. Xie, M. Huo, X. Ni, F. Shen, X. Huang, H. Sun, H. C. Walker, D. Adroja, D. Yu, B. Shen, L. He, K. Cao, and M. Wang, *arXiv 2401.12635* (2024).
  - [11] X. Chen, J. Choi, Z. Jiang, J. Mei, K. Jiang, J. Li, S. Agrestini, M. Garcia-Fernandez, X. Huang, H. Sun, D. Shen, M. Wang, J. Hu, Y. Lu, K.-J. Zhou, and D. Feng, *arXiv 2401.12657* (2024).
  - [12] Z. Dan, Y. Zhou, M. Huo, Y. Wang, L. Nie, M. Wang, T. Wu, and X. Chen, *arXiv 2401.12657* (2024).
  - [13] D. Takegami, K. Fujinuma, R. Nakamura, M. Yoshimura, K.-D. Tsuei, G. Wang, N. N. Wang, J.-G. Cheng, Y. Uwatoko, and T. Mizokawa, *Phys. Rev. B* **109**, 125119 (2024).
  - [14] Z. Luo, X. Hu, M. Wang, W. Wu, and D.-X. Yao, *Phys. Rev. Lett.* **131**, 126001 (2023).
  - [15] Y. Zhang, L.-F. Lin, A. Moreo, and E. Dagotto, *Phys.*

- Rev. B **108**, L180510 (2023).
- [16] V. Christiansson, F. Petocchi and P. Werner, *Phys. Rev. Lett.* **131**, 206501 (2023).
- [17] Q.-G. Yang, D. Wang, and Q.-H. Wang, *Phys. Rev. B* **108**, L140505 (2023).
- [18] H. Sakakibara, N. Kitamine, M. Ochi, and K. Kuroki, *Phys. Rev. Lett.* **132**, 106002 (2024).
- [19] Y. Shen, M. Qin, and G.-M. Zhang, *Chinese Phys. Lett.* **40**, 127401 (2023).
- [20] Y.-B. Liu, J.-W. Mei, F. Ye, W.-Q. Chen, and F. Yang, *Phys. Rev. Lett.* **131**, 236002 (2023).
- [21] Y. Zhang, L.-F. Lin, A. Moreo, T. A. Maier, and E. Dagotto, *Nat. Commun.* **15**, 2470 (2024).
- [22] Y.-F. Yang, G.-M. Zhang, and F.-C. Zhang, *Phys. Rev. B* **108**, L201108 (2023).
- [23] H. Oh and Y. H. Zhang, *Phys. Rev. B* **108**, 174511 (2023).
- [24] Z. Liao, L. Chen, G. Duan, Y. Wang, C. Liu, R. Yu, and Q. Si, *Phys. Rev. B* **108**, 214522 (2023).
- [25] Y. Cao, and Y.-F. Yang, *Phys. Rev. B* **109**, L081105 (2024).
- [26] F. Lechermann, J. Gondolf, S. Bötzel, and I. M. Eremin, *Phys. Rev. B* **108**, L201121 (2023).
- [27] D. A. Shilenko, and I. V. Leonov, *Phys. Rev. B* **108**, 125105 (2023).
- [28] K. Jiang, Z. Wang, and F. Zhang, *Chin. Phys. Lett.* **41**, 017402 (2024).
- [29] J. Huang, Z. D. Wang, and T. Zhou, *Phys. Rev. B* **108**, 174501 (2023).
- [30] Y. Zhang, L.-F. Lin, A. Moreo, T. A. Maier, and E. Dagotto, *Phys. Rev. B* **108**, 165141 (2023).
- [31] Q. Qin, and Y.-F. Yang, *Phys. Rev. B* **108**, L140504 (2023).
- [32] Y. Zhang, L.-F. Lin, A. Moreo, T. A. Maier, and E. Dagotto, *Phys. Rev. B* **109**, 045151 (2024).
- [33] T. Kaneko, H. Sakakibara, M. Ochi, and K. Kuroki, *Phys. Rev. B* **109**, 045154 (2024).
- [34] X.-Z. Qu, D.-W. Qu, J. Chen, C. Wu, F. Yang, W. Li, and G. Su, *Phys. Rev. Lett.* **132**, 036502 (2024).
- [35] C. Lu, Z. Pan, F. Yang, and C. Wu, *Phys. Rev. Lett.* **132**, 146002 (2024).
- [36] J. Li, P. Ma, H. Zhang, X. Huang, C. Huang, M. Huo, D. Hu, Z. Dong, C. He, J. Liao, X. Chen, T. Xie, H. Sun, M. Wang, *arXiv 2404.11369* (2024).
- [37] X. Chen, J. Zhang, A.S. Thind, S. Sharma, H. LaBollita, G. Peterson, H. Zheng, D. Phelan, A. S. Botana, R. F. Klie, and J. F. Mitchell, *J. Am. Chem. Soc.* **146**, 23640 (2024).
- [38] P. Puphal, P. Reiss, N. Enderlein, Y.-M. Wu, G. Khaliullin, V. Sundaramurthy, T. Priessnitz, M. Knauft, L. Richter, M. Isobe, P. A. van Aken, H. Takagi, B. Keimer, Y. E. Suyolcu, B. Wehinger, P. Hansmann, and M. Hepting, *arXiv 2312.07341* (2023).
- [39] H. Wang, L. Chen, A. Rutherford, H. Zhou, W. Xie, *Inorg. Chem.* **63**, 5020 (2024).
- [40] S. N. Abadi, K.-J. Xu, E. G. Lomeli, P. Puphal, M. Isobe, Y. Zhong, A. V. Fedorov, S.-K. Mo, M. Hashimoto, D.-H. Lu, B. Moritz, B. Keimer, T. P. Devereaux, M. Hepting, Z.-X. Shen, *arXiv 2402.07143* (2024).
- [41] J. Zhang, D. Phelan, A. S. Botana, Y.-S. Chen, H. Zheng, M. Krogstad, S. G. Wang, Y. Qiu, J. A. Rodriguez-Rivera, R. Osborn, S. Rosenkranz, M. R. Norman, and J. F. Mitchell, *Nat. Commun.* **11**, 6003 (2020).
- [42] A. M. Samarakoon, J. Strempler, J. Zhang, F. Ye, Y. Qiu, J.-W. Kim, H. Zheng, S. Rosenkranz, M. R. Norman, J. F. Mitchell, and D. Phelan, *Phys. Rev. X* **13**, 041018 (2023).
- [43] H. Sakakibara, M. Ochi, H. Nagata, Y. Ueki, H. Sakurai, R. Matsumoto, K. Terashima, K. Hirose, H. Ohta, M. Kato, Y. Takano, and K. Kuroki, *arXiv 2309.09462* (2023).
- [44] Q. Li, Y.-J. Zhang, Z.-N. Xiang, Y. Zhang, X. Zhu and H.-H. Wen, *Chinese Phys. Lett.* **41**, 017401 (2024).
- [45] Y. Zhu, E. Zhang, B. Pan, X. Chen, D. Peng, L. Chen, H. Ren, F. Liu, N. Li, Z. Xing, J. Han, J. Wang, D. Jia, H. Wo, Y. Gu, Y. Gu, L. Ji, W. Wang, H. Gou, Y. Shen, T. Ying, X. Chen, W. Yang, C. Zheng, Q. Zeng, J.-G. Guo, and J. Zhao, *arXiv 2311.07353* (2023).
- [46] M. Zhang, C. Pei, X. Du, Y. Cao, Q. Wang, J. Wu, Y. Li, Y. Zhao, C. Li, W. Cao, S. Zhu, Q. Zhang, N. Yu, P. Cheng, J. Zhao, Y. Chen, H. Guo, L. Yang, and Y. Qi, *arXiv 2311.07423* (2023).
- [47] J. Li, C. Chen, C. Huang, Y. Han, M. Huo, X. Huang, P. Ma, Z. Qiu, J. Chen, X. Hu, L. Chen, T. Xie, B. Shen, H. Sun, D. Yao, and M. Wang, *arXiv 2311.16763* (2023).
- [48] S. V. Streltsov and D. I. Khomskii, *Phys. Rev. B* **89**, 161112(R) (2014).
- [49] Y. Zhang, L. F. Lin, A. Moreo, and E. Dagotto, *Phys. Rev. B* **104**, L060102 (2021).
- [50] Y. Zhang, L.-F. Lin, A. Moreo, T. A. Maier, and E. Dagotto, *arXiv 2402.05285* (2024).
- [51] G. Kresse and J. Hafner, *Phys. Rev. B* **47**, 558 (1993).
- [52] G. Kresse and J. Furthmüller, *Phys. Rev. B* **54**, 11169 (1996).
- [53] P. E. Blöchl, *Phys. Rev. B* **50**, 17953 (1994).
- [54] J. P. Perdew, K. Burke, and M. Ernzerhof, *Phys. Rev. Lett.* **77**, 3865 (1996).
- [55] K. Momma and F. Izumi, *J. Appl. Crystallogr.* **44**, 1272 (2011).
- [56] Here, based on the lattice structure of the P4/mmm phase at 16 GPa [38], we fully relaxed the atomic positions until the Hellman-Feynman force on each atom was smaller than 0.001 eV/Å. In addition, we also studied the electronic structures by introducing additional Hubbard  $U$  effects by using the Dudarev's rotationally invariant formulation [57], where the low-energy physics picture does not change (more details can be found in the Supplemental Materials [58]).
- [57] S. L. Dudarev, G. A. Botton, S. Y. Savrasov, C. J. Humphreys, and A. P. Sutton, *Phys. Rev. B* **57**, 1505 (1998).
- [58] See Supplemental Material for method details and more results.
- [59] Y. Zhang, L.-F. Lin, W. Hu, A. Moreo, S. Dong, and E. Dagotto, *Phys. Rev. B* **102**, 195117 (2020).
- [60] A. A. Mostofi, J. R. Yates, Y. S. Lee, I. Souza, D. Vanderbilt, and N. Marzari, *Comput. Phys. Commun.* **178**, 685 (2007).
- [61] K. Kubo, *Phys. Rev. B* **75**, 224509 (2007).
- [62] S. Graser, T. A. Maier, P. J. Hirschfeld, and D. J. Scalapino, *New J. Phys.* **11**, 25016 (2009).
- [63] M. Altmeyer, D. Guterding, P. J. Hirschfeld, T. A. Maier, R. Valentí, and D. J. Scalapino, *Phys. Rev. B* **94**, 214515 (2016).
- [64] A. T. Rømer, T. A. Maier, A. Kreisel, I. Eremin, P. J. Hirschfeld, and B. M. Andersen, *Phys. Rev. Res.* **2**, 013108 (2020).